ACS OMEGA

http://pubs.acs.org/journal/acsodf

Article

Simultaneously Enhancing the Fire Retardancy and Heat Resistance of Stereo-Complex-Type Polylactic Acid

Yanlin Liu, Rui Wang,* Xiuqin Zhang,* Jing Zhang, Zhenfeng Dong, Tongyan Cui, Shuilian Wang, and Jianfei Wei

Cite This: *ACS Omega* 2022, 7, 22149−22160

Read Online

ACCESS | Metrics & More | Article Recommendations

ABSTRACT: Polylactic acid (PLA) is considered to be the material with great application potential in the 21st century which has aroused wide research interest. However, PLA is a highly flammable material and exhibits low heat distortion temperature, which greatly limits its application in many fields. In this work, aluminum diethyl phosphinate (ADP) and poly (D-lactic acid) (PDLA) are used to improve fire retardancy and heat resistance of poly (L-lactic acid) (PLLA). PLLA/PDLA with the presence of 15 wt % ADP exhibited the limiting oxygen index (LOI) value at 26%, and the peak heat release rate (pHRR) and total heat release decreased, respectively, by 14.03 and 24.42% from 500 to 429 kW/m^2 and 86 to 65 MJ/m^2. The melt dripping phenomenon was suppressed obviously. The addition of ADP realized the flame-retardant effect from both the condensed phase and gas phase. Moreover, the results showed that the addition of ADP promoted the formation of stereo crystals and increased the crystallization temperature to 175 °C. The heat distortion temperature (HDT) of the PLLA/PDLA sample with 15 wt % ADP can be as high as 170.4 °C, which marks significant improvement in the heat resistance of PLA. The mechanical property test results showed that ADP has little effect on the mechanical properties of the composites. This work opens a window to realize the heat-resistant and anti-dripping fire-retardant PLA.

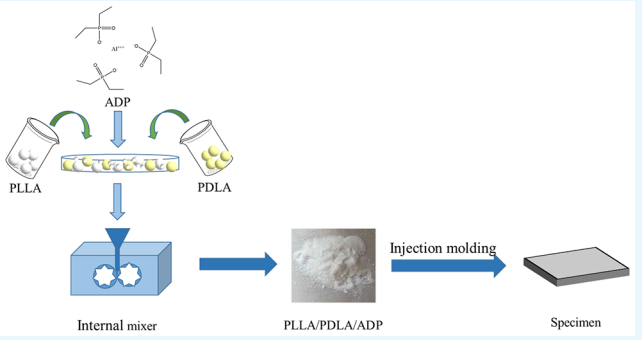

1. INTRODUCTION

Sustainability is the inevitable trend in material development. Products made from polylactic acid (PLA) can directly decompose after use.[1] Therefore, PLA materials that can achieve environmental protection and resource recycling are considered as one of the materials with the most potential and wide application prospects in the 21st century.[2,3] However, PLA materials generally have shortcomings such as low mechanical strength, poor toughness, slow crystallization rate, low crystallinity, and poor heat resistance [heat deformation temperature (HDT) is only 58 °C], which greatly limit their application fields.[4−6] In order to improve the heat resistance and flame retardancy of PLA, researchers have conducted a lot of studies.

The vicat softening temperature (VST) and HDT are usually used to evaluate the heat resistance of polymer materials. At present, there are three main methods to improve the heat resistance of PLA materials, including blending modification, chain structure modification, and crystal modification. Blending modification mainly includes polymer composite modification and nano modification. Qu et al.[7] reported that the blend of PLA and polycarbonate (PC) was prepared by melt processing in a twin-screw extruder. Ethylene-maleic anhydrideglycidyl methacrylate terpolymer (EMG) was used as a compatibilizer, and talc was added as a nucleating agent. The results showed that the addition of EMG and talc can improve the compatibility of PLA/PC. The HDT and crystallinity of PLA/PC blends increased, and the heat resistance was improved. Xu et al.[8] added graphene oxide (GO) into PLA, and found that GO effectively increased the HDT to 165 °C, and simultaneously reduced the oxygen permeability coefficient (P_{O_2}). The chain structure modification mainly includes copolymerization modification and cross-linking modification. Deng et al.[9] melt-blended the equimolar PLLA/PDLA blend with reactive poly (ethylene-methyl acrylate-glycidyl methacrylate) (E-MA-GMA) under the action of a catalyst, and the blended PLLA/PDLA three-dimensional crystal segment of PDLA is grafted to the E-MA-GMA main chain, thereby significantly improving the melt stability of SC-

Received: December 13, 2021
Accepted: April 20, 2022
Published: June 16, 2022

https://doi.org/10.1021/acsomega.1c07025
ACS Omega 2022, 7, 22149−22160

PLA and forming SC crystals with high crystallinity. Studies have shown that the E-MA-g-PLA chain can also be used as a compatibilizer to greatly enhance the interfacial adhesion. The VST increased from 151 to 201 °C, and the HDT is up to 174 °C. The impact strength increased from 45 to 65 kJ/m^2. Hongwei Bai et al.[10] prepared cross-linked PLLA/PDLA blend through melt mixing, with dicumyl peroxide (DCP) as a free radical initiator and triallyl isocyanurate (TAIC) as a cross-linking agent. It is found that the SC crystals formed in the cross-linked blend have excellent recrystallization ability and good melting stability. The blend exhibited excellent heat resistance. Crystallization modification mainly includes addition of the nucleating agent and modification in process technology. Zhang et al.[11] added a polyamide compound (TMC-328, abbreviated as TMC) as the nucleating agent. It was found that TMC showed an efficient nucleation effect, accelerating the crystallization rate, increasing the crystallinity and HDT. The above examples have greatly improved the heat resistance of PLA. There are also some nucleating agents that can promote the formation of the SC crystal in the blend of PLLA and PDLA. Song et al.[12] explored the influence of process conditions on the SC formation by changing the pressure and shear rate. It was found that the higher fluidity (corresponding higher shear rate) can promote the formation of SC crystals, while pressure showed an inhibitory effect. At present, the most popular method to improve the heat resistance of PLA materials is crystallization modification, among which the control of process conditions is more efficient. In order to maintain its biodegradability, researchers try to use bio-based materials for modification. Although it can meet some single improvement in PLA performance, the realization of high-performance heat-resistant PLA is still a current challenge.

PLA is a non-flame-retardant material, and its limiting oxygen index (LOI) is around 19−21%. It can only reach the V-2 grade in the UL-94 combustion test, accompanied by severe melting and dripping. The high flammability of PLA greatly limits its application in the fields of electronic appliances, automobile industry, and so forth. Therefore, it is imperative to improve the flame retardancy of PLA. The general method is the addition of flame retardants to form an isolation carbon layer after ignition, which can prevent the penetration of combustible gas (out) and oxygen (in). In addition, adding cross-linking nucleating agent or increasing melt viscosity can prevent or suppress the melt-dripping phenomena.[13] The flame-retardant methods are classified into incorporating additive fire retardants (FRs), copolymerization reaction, and surface modification. According to the elements, the additive FRs include halogen-based FRs, phosphorus-based FRs, nitrogen-based FRs, siloxane containing FRs, and so forth. Cen et al.[14] used chitosan and ZIF-8 supported GO (ZG) as flame retardants to prepare PLA composite films by solution blending. Studies have shown that ZG acts as a compatibilizer, effectively improving the compatibility of chitosan and PLA matrix. The ZnO derived from ZG has a significant catalytic effect on carbon formation and promotes the formation of a continuous and dense char layer, which significantly improves the flame retardancy of PLA. The LOI value of the PLA composite can reach 25.2%. Wang et al.[15] synthesized cross-linked flame-retardant PLA/ramie composites through direct polycondensation, followed by end group modification and cross-linking curing reaction. The reactive FR DOPO was used as the flame retardant. It was found that, with the increase of DOPO content, the LOI showed an increasing trend. When the DOPO content was 7 wt %, the LOI value of the composite material was the largest (25.2%). The presence of DOPO effectively inhibited the heat release of the material during the combustion process. The acid products from the DOPO decomposition can promote char formation, which inhibited the release of combustible gas and thus delayed the combustion process. Wang et al.[16] first used alkali/flame-retardant/silane coupling agent composite treatment to modify the surface of ramie fabric and then prepared the ramie reinforced PLA composite through a molding process. The ramie fabric/PLA composite material showed 1 cm of damage length upon ignition time of 12 s and 8.25 cm of damage length in 60 s combustion without dripping. Although the fire retardancy of the PLA composites have been greatly improved, simultaneously enhancing the fire retardancy and heat resistance is still challenged and plays an important role in the application of PLA.

In this work, aluminum diethyl phosphinate (ADP) is selected to simultaneously tailor the fire retardancy, crystallization behavior, and heat resistance of stereo-complex-type PLA. The effect of ADP on the property of PLA has been systematically studied, and the fire retardancy mechanism has been proposed. This work aims to prepare fire-retardant and heat-resistant PLA by a facile way.

2. MATERIALS AND METHODS

2.1. Materials. Poly(L-lactic acid) (PLLA, REVODE 190, optical purity > 99%, viscosity average molecular weight: 1.85 × 10^5) is provided by Hisun Biomaterials. Poly (D-lactic acid) (PDLA, D120, optical purity > 99%, viscosity average molecular weight: 1.59 × 10^5) is provided by TOTAL. ADP is provided by Guangzhou Xijia New Materials Co. Ltd.

2.2. Preparation of PLLA/PDLA Composites. PLLA, PDLA, and ADP were placed in the vacuum oven for 24 h at 80 °C to remove moisture. The mixtures containing 1:1 (mass ratio) of PLLA and PDLA with different mass fractions of ADP were added to an internal mixer (Haake, Thermo Fisher Scientific) for 5 min of blending at 190 °C. The rotation speed is at 60 rpm. The obtained white powder PLLA/PDLA/ADP samples is dried in a vacuum oven at 100 °C for 12 h and then injected into the mold using a plastic injection molding machine (JPH30). The temperature of the first zone of the screw is 250 °C, and the temperatures of following zones are 255, 265, 255, and 250 °C, respectively. The mold temperature is room temperature. The preparation for PLLA samples and PLLA/PDLA (PLLA/PDLA = 1:1) samples are carried out the same way without adding ADP or PDLA. For studying the heat resistance of pristine PLLA, PLLA/PDLA, and PLLA/PDLA/ADP15 samples, the powder obtained from internal mixer was injected [Thermo Fisher Scientific (China) Co., Ltd.] into the mold with optimal mold temperatures at 120 °C (30 min), 130 °C (2 min), and 170 °C (2 min), respectively (Table 1).

2.3. Characterizations and Measurements. *2.3.1. Differential Scanning Calorimeter.* The crystallization behavior of pure PLLA and its composites was studied through DSC (Q2000, TA Instruments) under N_2 atmosphere. In non-isothermal crystallization tests, the samples were heated to 250 °C at a rate of 30 °C/min and kept for 5 min to remove thermal history and cooled down to 30 °C at a rate of 10 °C/min. Then, the samples were reheated at a rate of 10 °C/min to 250 °C. The cooling curve and the second heating curve

https://doi.org/10.1021/acsomega.1c07025
ACS Omega 2022, 7, 22149−22160

Table 1. Composition of PLLA/PDLA/ADP Composites

sample name	PLLA (wt %)	PDLA (wt %)	ADP (wt %)
PLLA	100.0		
PLLA/PDLA	50.0	50.0	
PLLA/PDLA/ADP5	47.5	47.5	5.0
PLLA/PDLA/ADP10	45.0	45.0	10.0
PLLA/PDLA/ADP15	42.5	42.5	15.0
PLLA/PDLA/ADP20	40.0	40.0	20.0

were recorded. The following equations were utilized for calculating the crystallinity[17]

$$X_{HC} = \frac{\Delta H_{m,HC} - \Delta H_{cc}}{\Delta H^{0}_{m,HC}} \times 100\% \quad (1)$$

$$X_{SC} = \frac{\Delta H_{m,SC} - \Delta H_{cc}}{\Delta H^{0}_{m,SC} \times W_f} \times 100\% \quad (2)$$

Where W_f refers to the mass fraction of PLLA and PDLA, ΔH_{CC} is the cold crystallization enthalpy value during the differential scanning calorimetery (DSC) heating process, $\Delta H_{m,HC}$ refers to the melting enthalpy value of the HC crystals, and $\Delta H_{m,SC}$ is the melting enthalpy value of the SC crystals. $\Delta H_{m,HC}{}^{0}$ is the melting enthalpy of HC crystals of PLLA with 100% crystallinity (93 J g^{-1}). $\Delta H_{m,SC}{}^{0}$ is the melting enthalpy of SC crystals of PLLA/PDLA with 100% crystallinity (142 J g^{-1}).[18]

2.3.2. Thermogravimetric Analyzer. The thermal stability of the samples was tested by thermogravimetric analyzer (TGA) (Netzsch TG 209 F1) under N_2 atmosphere with a heating rate at 10 °C/min.

2.3.3. Limited Oxygen Index. The LOI value of the sample was tested with the US Dynisco oxygen index tester according to GB/T 2406.2-2009 standard. The size of the sample is 80 mm × 6.5 mm × 3 mm.

2.3.4. Cone Calorimetry Test. The test was carried out with the cone calorimeter (Fire Testing Technology Ltd). The heat radiation power was 35 kW/m^2, the sample size was 100 mm × 100 mm × 3 mm, and the test standard was based on ISO 5660-1.

2.3.5. Scanning Electron Microscopy. The surface morphology of the char layer was observed by scanning electron microscopy (SEM, JSM-7500F, Japan JEOL company). The acceleration voltage was 10 kV.

2.3.6. X-ray Diffraction. Crystal structure of the samples were analyzed by an X-ray diffractometer (DISCOVER-Bruker AG), using a Cu Kα radiation between the range 10−80°, and the scanning speed is 0.1°/s.

2.3.7. Temperature Deformation Test. The temperature deformation tests were carried out on a GTS-III thermal deformation performance measuring instrument (Shanghai Kailidi New Material Technology Co., Ltd). The measurements were carried out at a heating rate of 10 °C/min between the temperature range 25 and 250 °C.

2.3.8. Heat Distortion Temperature. The heat distortion temperature (HDT) tests were carried out on a microcomputer-controlled heat distortion vicat softening point tester (ZWK1302-B, MTS Industrial Systems (China) Co., Ltd.) in accordance with GB/T 1634-2004 standard with a sample size of 80 mm × 10 mm × 4 mm. The measurements were carried out in a methyl silicon oil bath at a heating rate of 2 °C/min, a span length of 64 mm, and a load of 0.46 MPa. The samples were prepared following the same procedure as the temperature deformation tests.

2.3.9. Mechanical Property Test. The tensile strength and elastic modulus of the samples were tested by a tensile tester (INSTRON5966, the US). The gauge length of the sample is 25 mm, and the tensile rate is 10 mm/min. The test standard is in accordance with GB/T 1040-1992.

2.3.10. X-ray Photoelectron Spectroscopy. The elemental analysis of the samples was carried out by an X-ray photoelectron spectrometer (XPS, Thermal escalab 250Xi) from Thermo Fisher Scientific. The target material was an aluminum target, and the emission voltage and current were 10 kV and 5 mA, respectively.

2.3.11. Thermogravimetric-Infrared Chromatography (TG-FTIR). Using the combination of infrared spectrometer and TGA, the sample blend powder obtained by internal mixing was heated from room temperature to 600 °C at a rate of 10 °C/min under nitrogen atmosphere. The temperature of the infrared thermogravimetric connection tube was 250 °C, the carrier gas was nitrogen, and the flow rate was 100 mL/min. The infrared scanning range is 400−4000 cm^{-1}, the resolution is 32 cm^{-1}, and an infrared spectrum was obtained by superimposing every 10 scans.

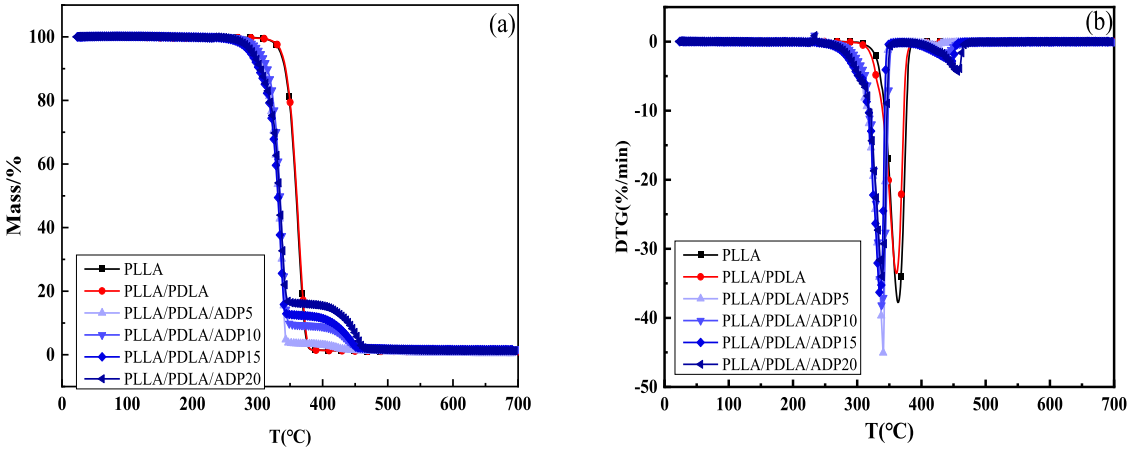

Figure 1. (a) TG curve and (b) DTG curve of PLLA, PLLA/PDLA, and PLLA/PDLA/ADP samples.

https://doi.org/10.1021/acsomega.1c07025
ACS Omega 2022, 7, 22149−22160

3. RESULTS AND DISCUSSION

3.1. Thermal Stability of PLLA/PDLA Composites. Figure 1 shows the TG test curves. Both PLLA and PLLA/PDLA samples exhibit one-step decomposition curve, the TG and DTG curves of which almost overlap. The thermal decomposition temperatures of two samples are around 335 and 337 °C, respectively, and the maximum thermal decomposition temperatures are about 363 and 360 °C, respectively. With the addition of ADP, PLLA/PDLA/ADP samples appear in two steps. The first step in the PLLA/PDLA/ADP sample is due to the decomposition of PLLA/PDLA, and the onset decomposition temperature (T_5 %) was slightly reduced.[19] The second plateau begins to drop at 406 °C. This attributed to the decomposition of ADP. The maximum weight loss rate of samples does not significantly change. After adding ADP, the remaining mass of the samples all increased, and the maximum thermal degradation rates (R_{max}) of the samples gradually decrease, indicating that degradation behavior of PLA was catalyzed by the metal aluminum ion. As shown in Table 2, the remaining mass fractions of samples with 10 wt % or more ADP are all over 1.2 wt %.

Table 2. TGA and DTG Data of PLLA, PLLA/PDLA, and PLLA/PDLA/ADP Samples

sample name	char residue (wt %)	T_5 % (°C)	T_{max} (°C)	R_{max} (%/min)[a]
PLLA	0	335	363	37.77
PLLA/PDLA	0	337	360	33.55
PLLA/PDLA/ADP5	0.46	295	339	38.22
PLLA/PDLA/ADP10	1.78	304	339	38.59
PLLA/PDLA/ADP15	1.61	289	336	36.68
PLLA/PDLA/ADP20	1.21	293	339	34.03

[a] R_{max}: maximum thermal degradation rate.

3.2. Fire Behavior of PLLA/PDLA Composites. The fire behavior of PLLA/PDLA/ADP samples was studied by LOI and cone calorimeter test (CCT). The LOI of the PLLA sample is only 19%, which is a non-flame-retardant material, while that of the PLLA/PDLA sample is increased to 21%. It indicates that the formation of SC crystals is beneficial to improve the fire retardancy of PLA. With the increase of the ADP content, the LOI of the samples gradually increases, up to 27% for PLLA/PDLA/ADP20, which demonstrated a great improvement in the flame-retardant performance. With the addition of 15 and 20 wt % of ADP, PLLA/PDLA/ADP samples are able to achieve an anti-dripping effect. As shown in Figure 2b,c, the digital photo of the PLLA/PDLA/ADP15 sample exhibits more residue and can better maintain their original shape rather than the melt dripping for the PLLA/PDLA/ADP5 sample.

The cone calorimetry test (CTT) is the bench scale tests which can measure many parameters such as heat release rate (HRR), total heat release (THR), effective heat combustion (EHC), and so forth. The results show that the addition of ADP reduced the HRR value of PLLA/PDLA (Figure 3). The HRR value of the sample with an ADP content of 15 and 20 wt % decreases to about 430 and 330 KW/m^2, respectively. Correspondingly, the THR value also reduced and the reduction degree is proportional to the amount of ADP. PLA is a degradable material, and the amount of smoke release is very small.[20] The PLLA/PDLA sample shows two peaks in the HRR curve, and the second peak reaches the peak value. After addition of ADP, the PLLA/PDLA/ADP20 sample reaches pHRR at around 80 s and the release of heat suppressed obviously. This is due to the effect of ADP which promotes the formation of the char residue and thus suppresses the further release of heat.[21] This indicates that the improvement of fire retardancy results from the condensed phase char formation. It can be evidenced by residue after combustion as shown in Table 3. The PLLA and PLLA/PDLA sample almost do not have any residues, while the samples after adding ADP exhibit the char barrier cover on the top. Moreover, the EHC values of PLLA/PDLA/ADP sample reduced from 20.21 to 17.18, representing the incomplete combustion and the potential gas phase mechanism from phosphorus-containing FR.[22] The char residues after CCT are shown in Table 3. With the increase of the ADP content, the char residue increases. The char residue of PLLA/PDLA/ADP20 reaches 9.78 wt %. This confirms that ADP plays the role in the condensed phase for flame-retardant mechanism. To further analyze the fire retardancy mechanism, the SEM was carried out for observing the morphology of the residue.

The PLLA sample left almost no residue after CCT (Figure 4a), which is not sufficient to protect the polymer from decomposition. However, the residue obtained from the PLLA/PDLA/ADP15 sample exhibits the greater amount of

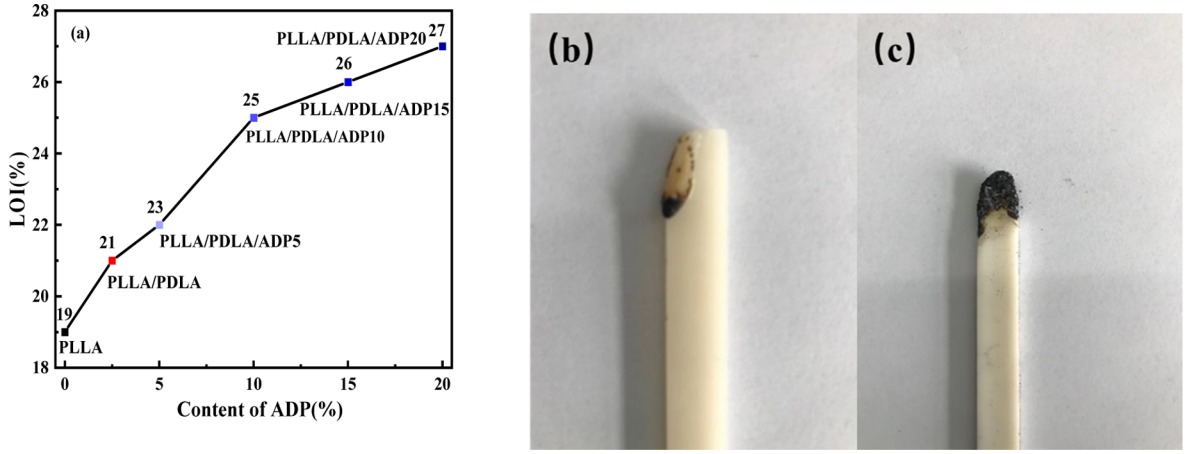

Figure 2. (a) LOI values of samples and digital photos of specimen for (b) PLLA/PDLA/ADP5 and (c) PLLA/PDLA/ADP15 after the LOI test.

https://doi.org/10.1021/acsomega.1c07025
ACS Omega 2022, 7, 22149−22160

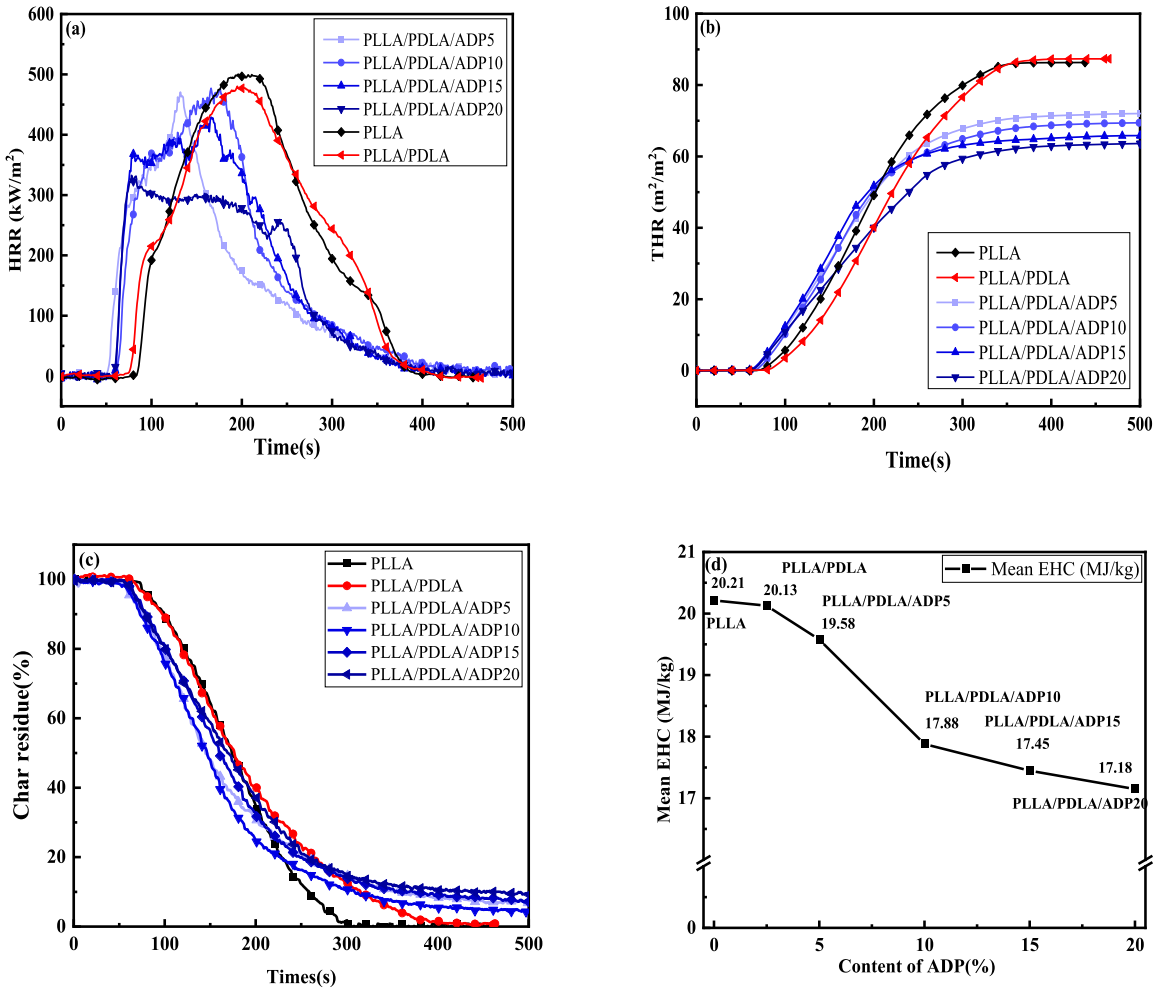

Figure 3. (a) Heat release rate; (b) THR; (c) char residue; and (d) mean EHC values curves of PLLA, PLLA/PDLA, and PLLA/PDLA/ADP samples.

Table 3. Data of Composite Samples After the CCT Test and LOI Test

sample name	PHRR (KW/m^2)	THR (MJ/m^2)	EHC (MJ/kg)	char residue (%)	LOI (%)
PLLA	500	86	20.21	0.0	19
PLLA/PDLA	480	87	20.13	0.0	21
PLLA/PDLA/ADP5	470	72	19.58	6.8	22
PLLA/PDLA/ADP10	477	69	17.88	4.3	25
PLLA/PDLA/ADP15	429	65	17.45	7.1	26
PLLA/PDLA/ADP20	331	63	17.18	9.8	27

char, which covers the entire sample holder (Figure 4b). Microscopic morphology of the residue shows the holes with different sizes and some bubbles (Figure 4c). Moreover, some of the bubbles were already being broken, while the rest remains closed. This is due to the decomposition of polymers, which release volatiles. The formation of the residue can be a barrier to partially block the oxygen and heat from contacting the underlying matrix.[23] The volatiles passed through the porous char structure, which extends the tortuous path and can play the great role in the condensed phase.[24]

XPS characterization was carried out to analyze the elemental composition of char residues of the PLLA/PDLA/ADP15 sample after the CTT. Figure 5 is the XPS spectrum of the carbon residue of the PLLA/PDLA/ADP15 sample. O element, C element, P element, and Al element, respectively, account for 33.43, 51.80, 8.61, and 6.15%. The C 1s peaks at 284.8, 285.7, 286.24, and 288.66 eV correspond to C−P, C−O, C−C−H, and C−C═O, respectively; the O 1s peaks correspond to O═C/O═P−C (531.62 eV), O−P (532.5 eV), and O−C (533.22 eV). The Al2p peaks (74.5−75.9 eV) corresponds to Al^{3+} in Al_2O_3, which proves that the composition of the white film on the surface of the carbon residue is Al_2O_3.[25] The dense Al_2O_3 can form a protective film on the surface of the carbon residue, which plays a flame-retardant role by blocking the inside−outside exchange of heat, gas-phase volatiles, and oxygen. Most of the P element remains in the carbon residue, which proves that Al and P elements in ADP are involved in the process of carbon residue formation.[26] ADP decomposes to generate free radical quenchers with flame-retardant properties such as PO$^•$, $PO_2^•$, HOPO$^•$, $HOPO_2^•$ and can effectively capture H$^•$ and $^•$OH produced by polymer combustion. This process can promote carbon

https://doi.org/10.1021/acsomega.1c07025
ACS Omega 2022, 7, 22149−22160

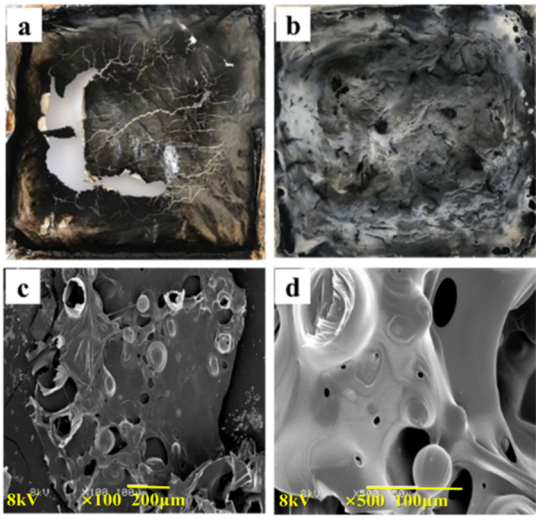

Figure 4. Digital photos of the sample after CCT for (a) PLLA, (b) PLLA/PDLA/ADP15, and SEM image of the residue from the PLLA/PDLA/ADP15 sample at different magnifications (c,d).

formation, realizing a flame-retardant mechanism from both the condensed phase and gas phase.

In order to further understand the effect of ADP on the gaseous products of thermal degradation of PLLA/PDLA, TG-FTIR was used to study the gas-phase products during decomposition of PLLA/PDLA/ADP15. The three-dimensional FTIR spectra of PLLA, PLLA/PDLA, and PLLA/PDLA/ADP15 are shown in Figure 6. It can be seen from the 3D graph that the intensity of absorption peaks for PLLA/PDLA/ADP15 decreased. This is due to the enhanced effect of ADP on the carbon residue, and the dense carbon residue is beneficial to reduce the gas release. The peaks for the PLLA and PLLA/PDLA appeared at 32 min (350 °C), while the peak for the PLLA/PDLA/ADP15 sample appeared at 28 min (310 °C). Figure 7 shows the infrared spectra of pyrolysis gases of PLLA, PLLA/PDLA, and PLLA/PDLA/ADP15 samples at different temperatures. In Figure 7a,b, at 280 °C, only the absorption peak of H_2O (3587 cm^{-1}) remaining in the air can be observed, indicating that no obvious decomposition reaction occurs before 280 °C. At 350 °C, the FT-IR spectra of gas-phase products became abundant, with CO (2183 and 2111 cm^{-1}), CO_2 (2350 and 2325 cm^{-1}), and hydrocarbons (3033 and 2111 cm^{-1}). The absorption peaks at 2739 and 2700 cm^{-1} were significantly enhanced. The stretching vibration peak of carbonyl (C═O) at 1740 cm^{-1} is mainly carbonyl in aliphatic lipids and carboxylic acids, indicating that the polymer has been degraded at this temperature.[27] The

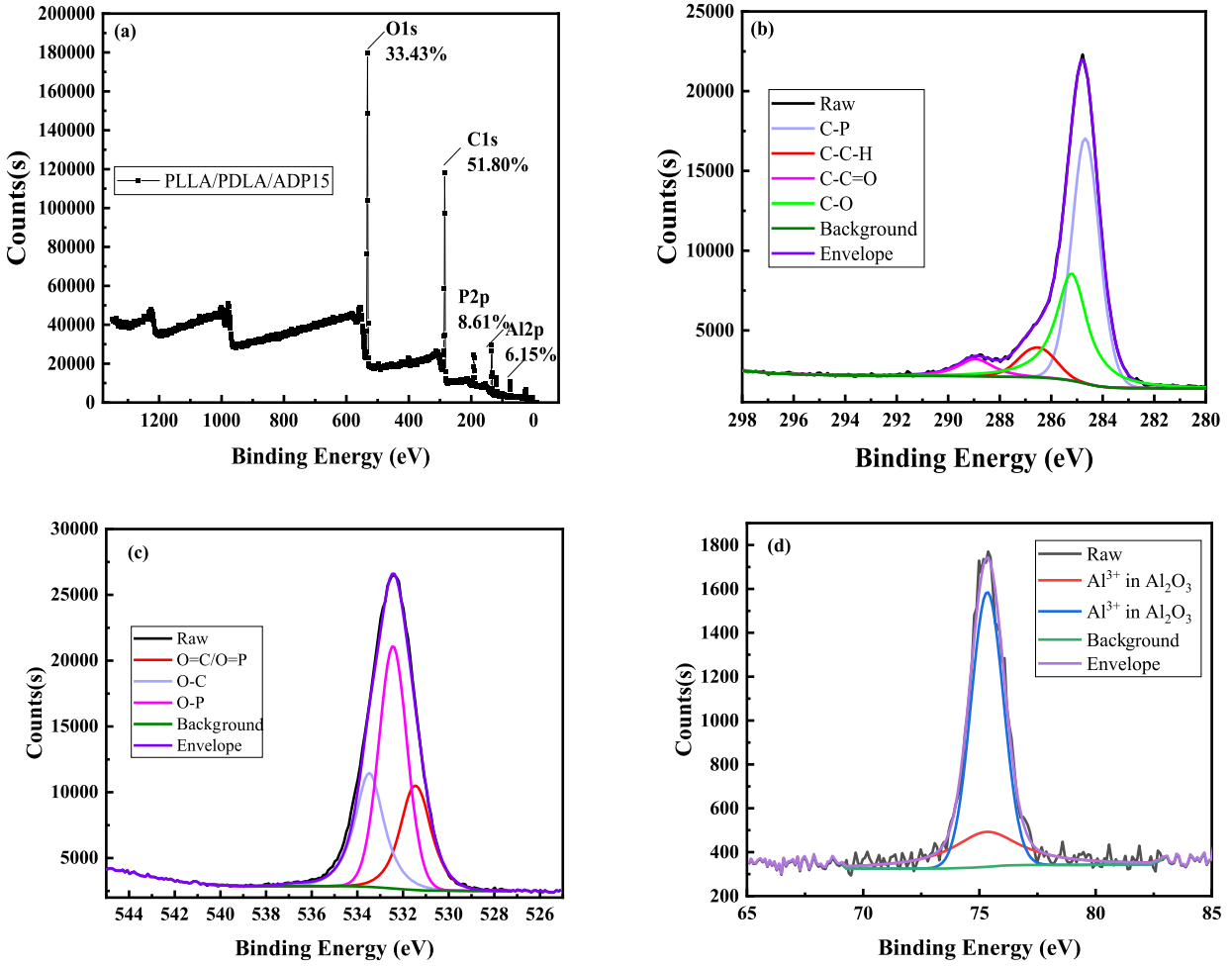

Figure 5. XPS spectrum of the carbon residue of PLLA/PDLA/ADP15. (a) XPS full spectrum; (b) C 1s spectrum; (c) O 1s spectrum; (d) Al 2p spectrum.

https://doi.org/10.1021/acsomega.1c07025
ACS Omega 2022, 7, 22149−22160

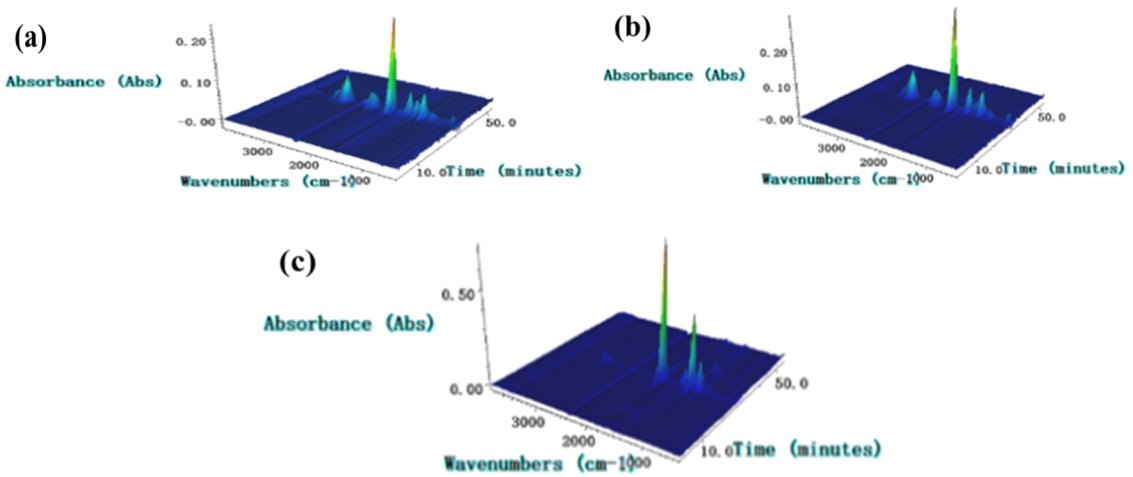

Figure 6. 3D FTIR spectra of samples in the TG-IR test; (a) PLLA, (b) PLLA/PDLA, and (c) PLLA/PDLA/ADP15.

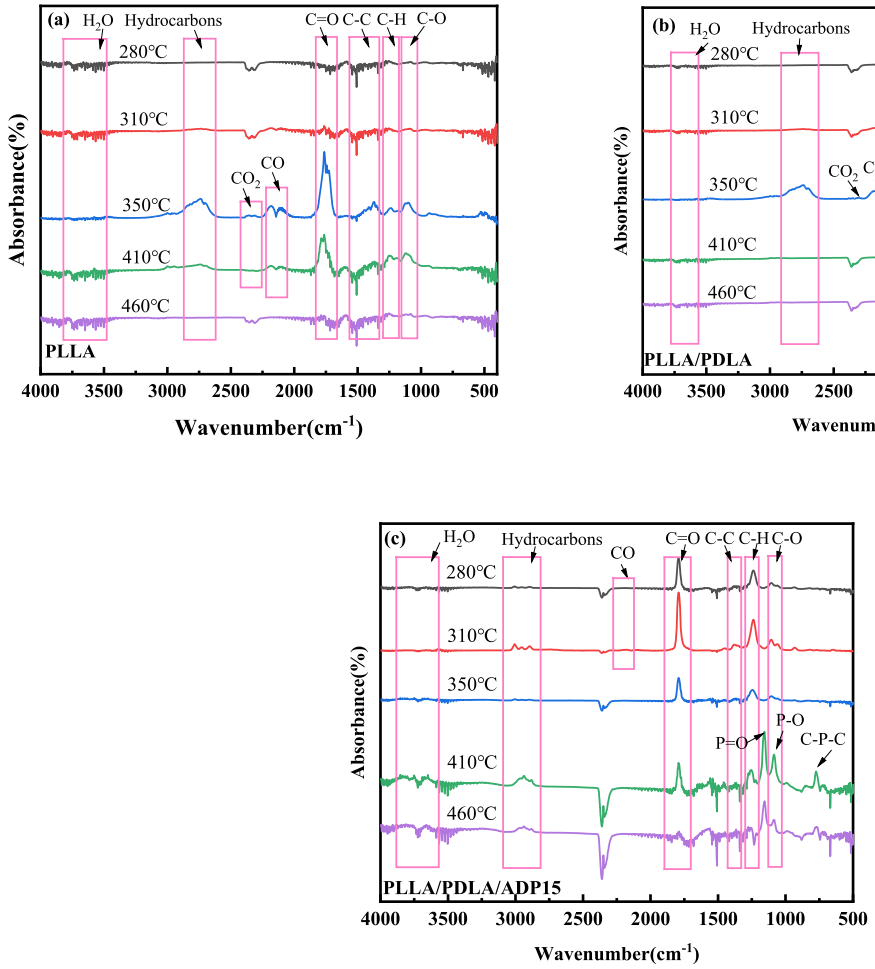

Figure 7. FTIR spectra of samples under the TG-IR test at different temperatures; (a) PLLA, (b) PLLA/PDLA, and (c) PLLA/PDLA/ADP15.

PLLA/PDLA/ADP15 sample showed stretching vibration peaks of carbonyl (C═O), hydrocarbon absorption peaks, C−O absorption peaks, and C−H absorption peaks at 280 °C. It is confirmed again that the addition of ADP promotes the decomposition of the polymer, and the absorption peak of CO only appears around 310 °C, and the absorption intensity is greatly reduced compared with the PLLA and PLLA/PDLA samples. There is almost no absorption peak of CO_2, which indicates that ADP can effectively inhibit the generation of harmful gases. At 410 °C, the peak at 1099 cm^{-1} is caused by the stretching vibration of P−O, the absorption peak of P═O at 1155 cm^{-1}, and the absorption peak of C−P−C at 772 cm^{-1}, indicating that ADP shows a cleavage at high temperature. The breakage of C−P−C bonds indicates that ADP is more likely decomposed into the gas phase, and ADP decomposes to generate free radical quenchers with flame-retardant properties such as $PO^{\bullet}$, $PO_2^{\bullet}$, $HOPO^{\bullet}$, $HOPO_2^{\bullet}$, and so forth, which trap the H· and HO·, thus realizing the gas-

https://doi.org/10.1021/acsomega.1c07025
ACS Omega 2022, 7, 22149−22160

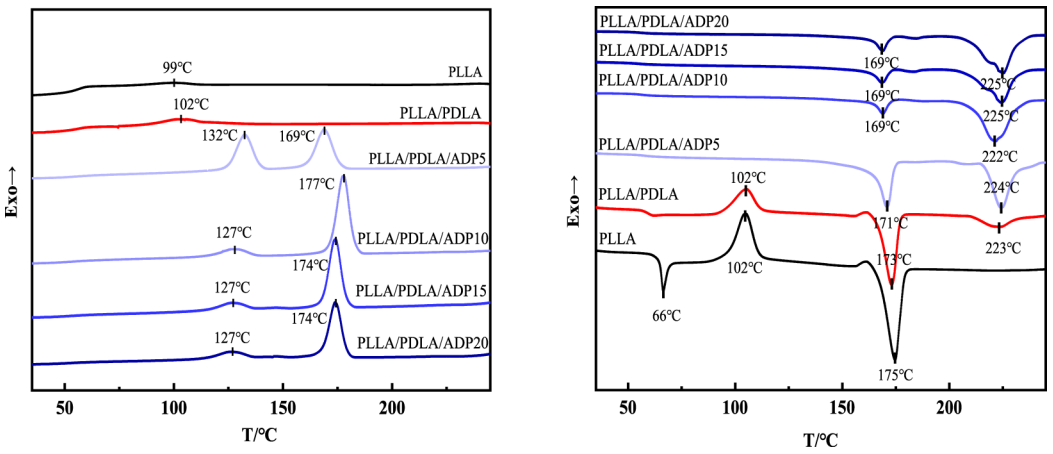

Figure 8. (a) DSC curve of the cooling scan; (b) DSC curve of the second heating scan of PLLA/PDLA and PLLA/PDLA/ADP samples.

Table 4. Enthalpy and Crystallinity of the Samples

sample name	ΔH_mSC (J g^{-1})	ΔH_mHC (J g^{-1})	ΔH_mSC (J g^{-1})	T_mHC (°C)	T_mSC (°C)	X_{HC} (%)	X_{SC} (%)
PLLA	26.37	46.22		175		21.21	
PLLA/PDLA	4.37	42.85	11.57	173	223	41.11	8.15
PLLA/PDLA/ADP5	0.00	42.15	23.21	171	224	47.40	17.21
PLLA/PDLA/ADP10	0.00	4.46	38.92	169	222	5.29	30.45
PLLA/PDLA/ADP15	0.00	3.82	37.72	169	225	4.79	31.25
PLLA/PDLA/ADP20	0.00	5.66	35.79	169	225	7.56	31.51

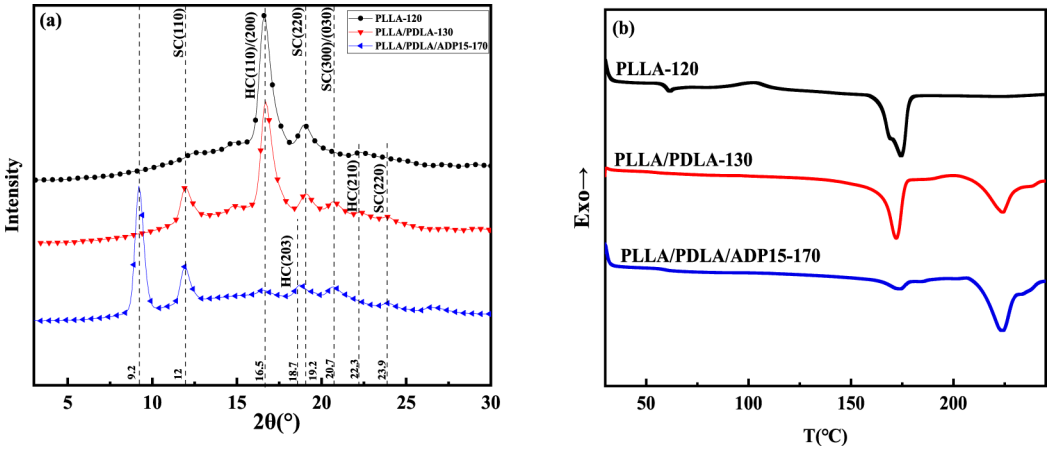

Figure 9. (a) X-ray diffraction spectrum and (b) DSC heating curve of PLLA, PLLA/PDLA, and PLLA/PDLA/ADP samples subjected to isothermal treatment at a suitable temperature.

phase flame-retardant effect. The absorption peak intensities of P−O, P═O, and C−P−C decreased at 460 °C.

3.3. Crystallization Behavior of PLLA/PDLA Composites. Figure 8a,b shows the cooling and second heating curves of PLLA, PLLA/PDLA, and PLLA/PDLA/ADP, respectively. The results showed that during the first cooling process of the PLLA sample, the crystallization peak is very weak around 99 °C. An obvious glass transition temperature appears at 66 °C, the cold crystallization temperature is at 102 °C, and the melting point is at 175 °C. The PLLA/PDLA blend shows a small crystallization peak at 102 °C. The samples with the presence of ADP showed crystallization peaks at around 130 and 170 °C. With the increase of the ADP content, the enthalpy of crystallization peak at 170 °C increases, while the crystallization peak near 130 °C weakens. According to the previously reported references, the crystallization peak near 130 °C is related to HC crystals and that near 170 °C is related to SC crystals.[28] The corresponding crystallization temperatures and crystallization enthalpies are shown in Figure 8a and Table 4. With the addition of 5 wt % of ADP, the crystallization temperature of SC crystals is 169 °C, and the crystallization enthalpy of SC is 23.21 J g^{-1}. When the content of ADP increased to 10 wt %, the crystallization temperature of SC crystals increases from 169 to 177 °C, and the crystallization enthalpy increases from 23.21 to 38.92 J g^{-1}. However, further increasing the content of ADP, the effect of ADP on the crystallization temperature and enthalpy SC crystals is limited. Figure 8b also shows the effect of ADP on the crystallization of PLLA/PDLA. Due to the low crystallinity of the PLLA/PDLA in the cooling process, a cold crystallization peak appears at 102 °C during the second heating process. The PLLA/PDLA with the presence of ADP

https://doi.org/10.1021/acsomega.1c07025
ACS Omega 2022, 7, 22149−22160

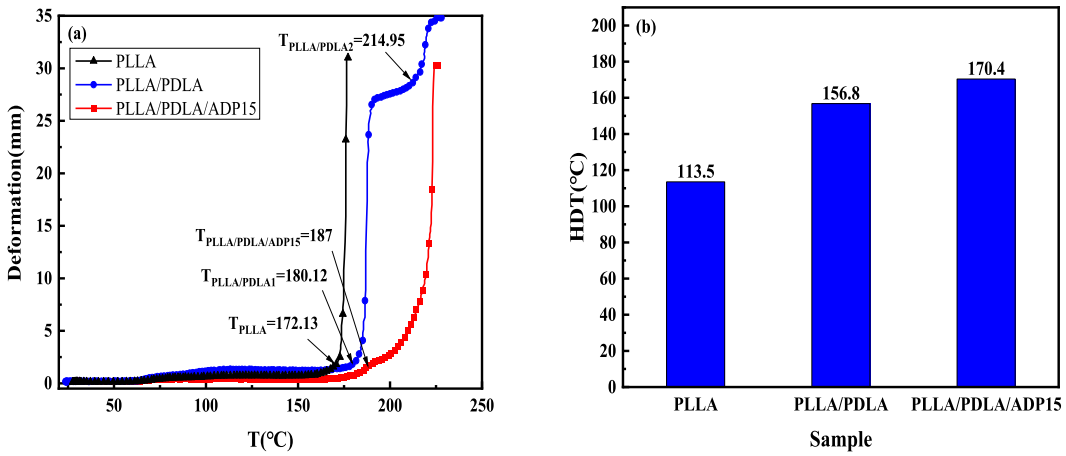

Figure 10. (a) Temperature−deformation curve and (b) HDT of suitable temperature processing sample.

does not show a cold crystallization peak.[29] The melting point and crystallinity of the formed SC and HC crystals are shown in Table 4. With the decrease of the mass fraction of PLLA, the melting point of the HC crystals of the sample decreases, which is due to the decrease of the optical purity. The PLLA/PDLA blend is mainly HC crystals with a crystallinity of 41.11%. The addition of 10 wt % ADP increased the crystallinity of SC to 30.45, compared with 8.15% of PLLA/PDLA, and the content of HC crystals decreased from 41.11 to 5.29%. More ADP over 10 wt % did not further increase the content of SC crystals. The above results show that when the content of ADP reaches 10 wt %, the formation of SC crystals in the blend can be effectively improved. Combination with research on the flame-retardant properties of PLLA/PDLA/ADP blends, it is concluded that the addition of 15 wt % ADP can make PLLA/PDLA blends obtain the best flame-retardant properties and SC crystallization properties.[30]

3.4. Analysis of the Crystallization and Heat Resistance of the Sample. The crystallization properties of the material affect the heat resistance of the material. The PLLA/PDLA/ADP15 was selected in this work to gain insights into the relationship between its crystallization performance and heat resistance. The fully crystallized sample, named as PLLA/PDLA/ADP15-170, was obtained by using a suitable mold temperature (170 °C, 2 min). For comparison, PLLA and PLLA/PDLA samples were also prepared by the injection machine with optimal condition, with the mold temperatures at 120 °C (30 min) and 130 °C (2 min), respectively. Their crystallization performances are shown in Figure 9.

In Figure 9a, the diffraction peak of sample PLLA/PDLA/ADP15-170 at 2θ = 9.2° is the crystalline peak of ADP. The PLLA sample has a high and sharp diffraction peak at 2θ = 16.5°, which belongs to the characteristic diffraction of the crystal plane (110)/(200) of the HC crystals. This indicates the formation of a large amount of HC crystals with crystallinity of 39.64%, as shown in the DSC curve (Figure 9b). Apart from the characteristic crystal plane (110)/(200) of the HC crystals, the PLLA/PDLA sample also shows a few small diffraction peaks at 2θ = 12, 19.2, and 20.7°, which, respectively, belong to the characteristic crystal planes (110), (220), and (300)/(030) of SC crystals.[31] Combined with the DSC curves in Figure 9b, it can be concluded that there are a large number of HC crystals (35.8%) and a small amount of SC crystals (22.4%) within the PLLA/PDLA sample. However, for the PLLA/PDLA/ADP15-170 sample, there is only a small characteristic diffraction peaks of HC crystals (5.09%) while that of SC crystals is strong (36.57%) (Figure 9 b). The above results show that by adjusting processing conditions such as mold temperature, the PLLA/PDLA/ADP15 sample can form more SC crystals during the injection molding process.[32]

Figure 10a shows the temperature−deformation curve of samples. The high crystallinity of the polymer will lead to a small deformation due to the chain segment being bound in the glass transition temperature region. With the temperature increase, the PLLA sample has an inflection point at 172 °C, at which the deformation increases rapidly resulted from the melting of the HC crystals. The PLLA/PDLA sample has the first inflection point at 184 °C which increases by 12 °C than that of PLLA and followed by the second inflection point at 215 °C. The two inflection points are, respectively, related to the melting points of the HC crystals and the SC crystals.[33] Due to the SC crystal domains in the PLLA/PDLA/ADP15 samples, the deformation temperature curve exhibits an inflection point at 218 °C. Therefore, the existence of SC crystals improves the heat resistance of PLLA during the heating process.

The HDT as a commonly used characterization method for the heat resistance of materials has been carried out, as shown in Figure 10b.[34] The HDT of the PLLA is only 113.5 °C. The HDT of the PLLA/PDLA and PLLA/PDLA/ADP15 samples improve to 156.8 °C and 170.4 °C, respectively. The optimal sample is 50.13% higher than that of the PLLA sample. Compared with the previously reported heat resistance of PLA, the improvement of HDT in this work is significant, which demonstrate that the heat resistance of the PLLA has been proofed (Table 5).

3.5. Mechanical Property. The mechanical properties of materials are important indicators to guide the spinnability of

Table 5. Comparison Study of HDT and Heat Resistance Property of PLA Composites between This work and Previously Reported Literature

researchers	system	X_{SC} (%)	T_mSC (°C)	HDT (°C)
Luo, et al.[35]	PLLA/PDLA/PEG	53.94	218.7	
Boonluksiri, et al.[36]	PLLA/PDLA (heating 80 °C)	10.10	224.8	164.0
this work	PLLA/PDLA/ADP15 (heating170 °C)	31.25	225.0	170.4

https://doi.org/10.1021/acsomega.1c07025
ACS Omega 2022, 7, 22149−22160

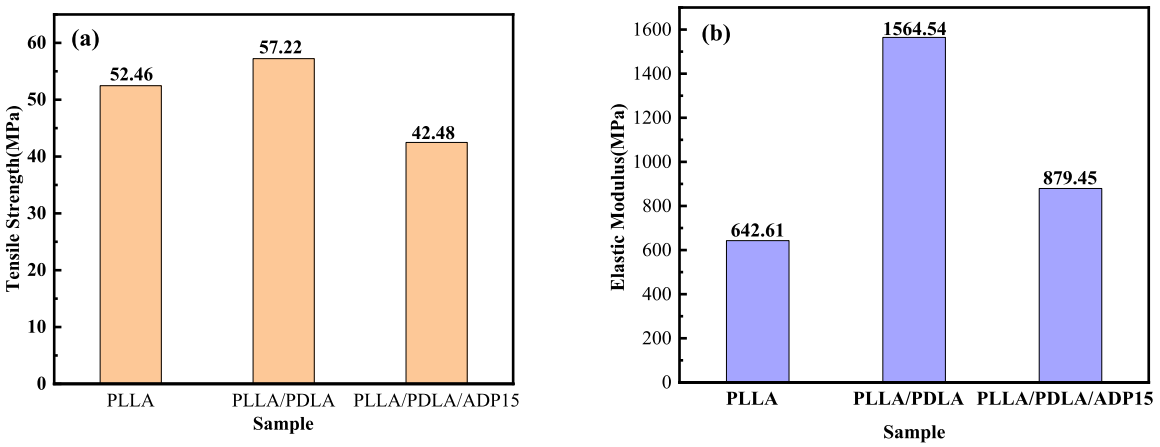

Figure 11. Mechanical properties of samples: (a) tensile strength; (b) elastic modulus.

materials. In order to explore the spinnability of the composites, the tensile properties of PLLA, PLLA/PDLA, and PLLA/PDLA/ADP15 were tested. The tensile strength and elastic modulus of the samples are shown in Figure 11. The tensile strength of the PLLA sample is 52.46 MPa, and the elastic modulus is 642.61 MPa. Compared with the PLLA sample, the mechanical properties of PLLA/PDLA increased to 57.22 MPa (tensile strength) and to 1564.54 MPa (elastic modulus). Intermolecular crystallization will increase molecular chain entanglement. The entanglement junction results in better mechanical properties. On the other hand, the stereo-complex formed finer crystallites, while PLLA formed large-sized spherulites due to low molecular chain density. It was the difference in the microphase structure between PLLA and the stereo-complex that led to their different mechanical properties.[37] However, the tensile strength and elastic modulus of the PLLA/PDLA/ADP15 sample are 42.48 and 879.45 MPa, respectively. The reason is that the addition of ADP can accelerate the crystallization rate and promote crystallization. The increased crystallinity and regularity can lead to improved mechanical properties. However, the mass fraction of the flame retardant in the system reaches 15 wt %, and it is easy to agglomerate in the matrix, resulting in brittle fracture. Further research on this aspect is required in the future.

4. CONCLUSIONS

To summarize, ADP and PDLA are used to simultaneously enhance the fire retardancy and heat resistance of PLLA. The addition of 15 wt % ADP in PLLA/PDLA improves the LOI to 26% and its composites exhibited 14.03 and 24.42% reduction in pHRR and THR, respectively. The combination of both the gas phase with decreased EHC value and condensed phase through char formation has been proved simultaneously effective in this work. Besides, the crystallization performance of the PLLA/PDLA/ADP sample has been greatly enhanced by accelerating the crystallization rate. Moreover, the addition of ADP is beneficial to the formation of SC crystals. The melting points of PLLA/PDLA/ADP15 sample can reach up to 225 °C. Correspondingly, the HDT of the PLLA/PDLA/ADP15 sample was 50.13% higher than that of the pure PLLA sample due to the dominant SC crystals. The addition of 15 wt % ADP has little effect on the mechanical properties of the composites. This work paves a facile pathway to the preparation of fire-retardant and heat-resistant PLA.

AUTHOR INFORMATION

Corresponding Authors

Rui Wang − *Beijing Institute of Fashion Technology, Beijing 10029, China; Beijing Key Laboratory of Clothing Materials R&D and Assessment, Beijing Engineering Research Center of Textile Nano Fiber, Beijing Institute of Fashion Technology, Beijing 100029, China;* orcid.org/0000-0001-5886-3261; Email: clywangrui@bift.edu.cn

Xiuqin Zhang − *Beijing Institute of Fashion Technology, Beijing 10029, China; Beijing Key Laboratory of Clothing Materials R&D and Assessment, Beijing Engineering Research Center of Textile Nano Fiber, Beijing Institute of Fashion Technology, Beijing 100029, China;* orcid.org/0000-0002-8687-4280; Email: clyzxq@bift.edu.cn

Authors

Yanlin Liu − *Beijing Institute of Fashion Technology, Beijing 10029, China;* orcid.org/0000-0001-6384-8939

Jing Zhang − *Beijing Institute of Fashion Technology, Beijing 10029, China; Beijing Key Laboratory of Clothing Materials R&D and Assessment, Beijing Engineering Research Center of Textile Nano Fiber, Beijing Institute of Fashion Technology, Beijing 100029, China*

Zhenfeng Dong − *Beijing Institute of Fashion Technology, Beijing 10029, China; Beijing Key Laboratory of Clothing Materials R&D and Assessment, Beijing Engineering Research Center of Textile Nano Fiber, Beijing Institute of Fashion Technology, Beijing 100029, China*

Tongyan Cui − *Beijing Institute of Fashion Technology, Beijing 10029, China*

Shuilian Wang − *Beijing Institute of Fashion Technology, Beijing 10029, China*

Jianfei Wei − *Beijing Institute of Fashion Technology, Beijing 10029, China; Beijing Key Laboratory of Clothing Materials R&D and Assessment, Beijing Engineering Research Center of Textile Nano Fiber, Beijing Institute of Fashion Technology, Beijing 100029, China;* orcid.org/0000-0003-4834-8623

Complete contact information is available at: https://pubs.acs.org/10.1021/acsomega.1c07025

Author Contributions

Y.L., J.Z., X.Z., J.W., and R.W. conceived the study and designed the experiments. Y.L. completed the melt spinning with the assistance of Z.D. Y.L., T.C., and S.W. wrote the manuscript with the assistance of all other co-author-

https://doi.org/10.1021/acsomega.1c07025
ACS Omega 2022, 7, 22149−22160

s.Conceptualization, Y.L., J.Z., X.Z., and R.W.; methodology, Y.L., Z.D., T.C., and S.W.; software, Y.L.; validation, Y.L., J.Z., X.Z., and R.W.; formal analysis, Y.L.; investigation, Y.L.; resources, R.W.; data curation, Y.L.; writing—original draft preparation, Y.L.; writing—review and editing, Y.L., J.Z., X.Z., and R.W.; visualization, Y.L.; supervision, R.W.; project administration, R.W.; and funding acquisition, R.W. All authors have read and agreed to the published version of the manuscript.

Notes

The authors declare no competing financial interest.

■ ACKNOWLEDGMENTS

This work was financially supported by National Key R&D Program of China; Beijing Scholars Program, grant number (2017YFB0309002) and (RCQJ20303). Thanks to the teachers of the project team for their guidance on the subject. Thanks to the students for their contributions and help to the subject experiment. Thanks to the foundation project team [National Key R&D Program of China; Beijing Scholars Program, grant number (2017YFB0309002) and (RCQJ20303)] for supporting this topic.

■ REFERENCES

(1) Yuhan, Z.; Lili, D.; Lei, C.; Wen, L.; Peijin, Z. Research development of PLA/plant fiber composite. *Chem. Ind. Times* **2018**, *32*, 39−42.

(2) Xiao, P.; Mingqiu, Q.; Junming, D. Development of poly (lactic acid) fibers at home and abroad. *Synth. Technol. Appl.* **2017**, *32*, 32−37.

(3) Huijuan, W.; Lijuan, Y. Research progress of PLA composites. *China Synth. Resin Plast.* **2017**, *34*, 88−92.

(4) Jie, C.; Rongrong, H.; Huanyu, L.; Youjia, D.; Yongqiang, Z.; Fanlong, J. Research progress on heat resistance modification of poly (lactic acid). *Plast. Sci. Technol.* **2018**, *46*, 115−119.

(5) He, S.; Hongwei, B.; Dongyu, B.; Yilong, J.; Qin, Z.; Qiang, F. A promising strategy for fabricating high-performance stereocomplex-type polylactide products via carbon nanotubes-assisted low-temperature sintering. *Polymer* **2019**, *162*, 50−57.

(6) Pan, P.; Jianna, B.; Lili, H.; Qing, X.; Guorong, S.; Yongzhong, B. Stereocomplexation of highmolecular-weight enantiomeric poly(lactic acid)s enhanced by miscible polymer blending with hydrogenbond interactions. *Polymer* **2016**, *98*, 80−87.

(7) Qu, Z.; Xiaoyue, H.; Xiaoxia, P.; Juan, B. Effect of compatibilizer and nucleation agent on the properties of poly(lactic acid)/polycarbonate (PLA/PC) blends. *Polym. Sci., Ser. A* **2018**, *60*, 499−506.

(8) Xu, H.; Duo, W.; Xi, Y.; Xie, L.; Hakkarainen, M. Thermostable and impermeable "Nano-Barrier Walls" constructed by poly(lactic acid) stereocomplex crystal decorated graphene oxide Nanosheets. *Macromolecules* **2015**, *48*, 2127−2137.

(9) Deng, S.; Bai, H.; Liu, Z.; Zhang, Q.; Fu, Q. Toward supertough and heat-resistant stereocomplex type polylactide/elastomer blends with impressive melt stability via in situ formation of graft copolymer during one-pot reactive melt blending. *Macromolecules* **2019**, *52*, 1718.

(10) Bai, H.; Huili, L.; Dongyu, B.; Qin, Z.; Ke, W.; Hua, D.; Feng, C.; Qiang, F. Enhancing the melt stability of polylactide stereocomplexes using a solid-state cross-linking strategy during a melt-blending process. *Poly. Chem.* **2014**, *5*, 5985−5993.

(11) Zhang, X.; Lingyan, M.; Gen, L.; Ningning, L.; Jing, Z.; Zhiguo, Z.; Rui, W. Effect of nucleating agents on the crystallization behavior and heat resistance of poly(l-lactide). *J. Appl. Polym. Sci.* **2015**, *133*, 42999.

(12) Yingnan, S.; Jun, L.; Zhongming, L. *Study on the crystallization behavior of polylactic acid stereocomplex (SC) induced by flow under pressure field*; China Offshore Platform, 2017.

(13) Rui, W.; Anying, Z.; Zhenfeng, D.; Xiuqin, Z.; Zhiguo, Z. Polylactic acid fiber gains flame retardancy. *Textil. Sci. Res.* **2019**, *11*, 70−71.

(14) Xinhao, C.; Mi, Z.; Qin, M.; Jianxiong, Y.; Xinlong, W. The Flame-Retardant Polyactic Acid Composite with MOFs@ GO and Chitosan. *Plastics* **2019**, *48*, 32−35.

(15) Jiao, W.; Xie, C.; Xiaoyan, L.; Naiwen, Z.; Jianbo, L.; Jie, R. Preparation and Properties of Flame Retardant Cross-Linked Polylactic Acid/Ramie Composite. *Plastics* **2018**, *47*, 1−4.

(16) Wang, C.; Ren, Z. L.; Li, S.; Wang, R. Effect of surface modification on properties of mechanical and flame retardant of ramie fabrics reinforced thermosetting polylactic acid composities. *Acta Mater. Compositae Sin.* **2015**, *32*, 444−450.

(17) Meirui, F.; Zhenwei, L.; Dongyu, B.; Fangwei, L.; Hongwei, B.; Qin, Z.; Qiang, F. Low-Temperature Sintering of Stereocomplex-Type Polylactide Nascent Powder. *Macromol. Mater. Eng.* **2018**, *303*, 1800178.

(18) Pan, P.; Bao, J.; Han, L.; Xie, Q.; Shan, G.; Bao, Y. Stereocomplexation of high-molecular-weight enantiomeric Poly-(lactic acid)s enhanced by miscible polymer blending with hydrogen bond interactions. *Polymer* **2016**, *98*, 80.

(19) Zhang, L.; Liu, W.; Wen, X.; Chen, J.; Zhao, C.; Castillo Rodríguez, M.; Yang, L.; Zhang, X.-Q.; Wang, R.; Wang, D.-Y. Electrospun Submicron NiO Fibers Combined with Nanosized Carbon Black as Reinforcement for Multi-functional Poly(lactic acid) Composites. *Composites, Part A* **2019**, *129*, 105662.

(20) Li, Z.; Daniel, F. E.; Alejandro, J. G.; De-yi, W. Natural halloysite nanotube based functionalized nanohybrid assembled via phosphorus-containing slow release method: A highly efficient way to impart flame retardancy to polylactide. *Eur. Polym. J.* **2017**, *93*, 458−470.

(21) Zhang, L.; Siqi, C.; Ye-tang, P.; Shuidong, Z.; Shibin, N.; Ping, W.; Xiuqin, Z.; Rui, W.; De-yi, W. Nickel Metal−Organic Framework Derived Hierarchically Mesoporous Nickel Phosphate toward Smoke Suppression and Mechanical Enhancement of Intumescent Flame Retardant Wood Fiber/Poly(lactic acid) Composites. *ACS Sustainable Chem. Eng.* **2019**, *7*, 9272−9280.

(22) Li, C.; Xia, L.; Chao, M.; Juan, L. Highly efficient flame retardant poly(lactic acid) using imidazole phosphate poly(ionic liquid). *Polym. Adv. Technol.* **2020**, *31*, 1765.

(23) Zhai, G.; Jialiang, Z.; Hengxue, X.; Mugaanire, I.; Senlong, Y.; Weinan, P.; Lili, L.; Meifang, Z. *Prog. Nat. Sci.: Mater. Int.* **2021**, *31*, 239.

(24) Cao, X.; Chi, X.; Deng, X.; Liu, T.; Yu, B.; Wang, B.; Yuen, A. C. Y.; Wu, W.; Li, R. K. Y. Synergistic effect of flame retardants and graphitic carbon nitride on flame retardancy of polylactide composites. *Polym. Adv. Technol.* **2020**, *31*, 1661.

(25) Jiang, H.; Mingshu, B.; Wei, G. Suppression mechanism of Al dust explosion by melamine polyphosphate and melamine cyanurate. *J. Hazard. Mater.* **2020**, *386*, 121648.

(26) Cao, X.; Chi, X.; Deng, X.; et al. Synergistic effect of flame retardants and graphitic carbon nitride on flame retardancy of polylactide composites. *Polym. Adv. Technol.* **2020**, *31*, 1661.

(27) Liu, L.; Xu, Y.; Di, Y.; Xu, M.; Pan, Y.; Li, B. Simultaneously enhancing the fire retardancy and crystallization rate of biodegradable polylactic acid with piperazine-1,4-diylbis(diphenylphosphine oxide). *Composites, Part B* **2020**, *202*, 108407.

(28) Luo, C.; Minrui, Y.; Wei, X.; Jingjing, Y.; Yan, W.; Weixing, C.; Xia, H. Relationship between the crystallization behavior of PEG and stereocomplex crystallization of PLLA/PDLA. *Polym. Int.* **2018**, *67*, 313−321.

(29) Liu, H.; Zhou, W.; Chen, P.; Bai, D.; Cai, Y.; Chen, J. A novel aryl hydrazide nucleator to effectively promote stereocomplex crystallization in high-molecular-weight poly(L-lactide)/poly(D-lactide) blends. *Polymer* **2020**, *210*, 122873.

(30) Gupta, A.; William, S.; Gregory, T.; Schueneman, E. A. M. Lignin-coated cellulose nanocrystals as promising nucleating agent for poly(lactic acid). *J. Therm. Anal. Calorim.* **2016**, *126*, 1243−1251.

https://doi.org/10.1021/acsomega.1c07025
ACS Omega 2022, 7, 22149−22160

(31) Pan, P.; Bao, J.; Han, L.; Xie, Q.; Shan, G.; Bao, Y. Stereocomplexation of high-molecular-weight enantiomeric poly(lactic acid)s enhanced by miscible polymer blending with hydrogen bond interactions. *Polymer* **2016**, *98*, 80−87.
(32) Zhang, X.; Lingyan, M.; Gen, L.; Ningning, L.; Jing, Z.; Zhiguo, Z.; Rui, W. Effect of nucleating agents on the crystallization behavior and heat resistance of poly(l -lactide). *J. Therm. Anal. Calorim.* **2016**, *133*, 42999.
(33) Zhao, C.; Miaomiao, Y.; Qicheng, F.; Guoxiang, Z.; Jinchun, L. The role of cold crystallization of homochiral crystallites in the superb heat resistant poly(lactic acid). *Polym. Adv. Technol.* **2020**, *31*, 1077−1087.
(34) Qu, Z.; Xiaoyue, H.; Xiaoxia, P.; Juan, B. Effect of Compatibilizer and Nucleation Agent on the Properties of Poly(lactic acid)/Polycarbonate (PLA/PC) Blends. *Polym. Sci., Ser. A* **2018**, *60*, 499−506.
(35) Luo, C.; Minrui, Y.; Wei, X.; et al. Relationship between the crystallization behavior of PEG and stereocomplex crystallization of PLLA/PDLA. *Polym. Int.* **2018**, *67*, 313−321.
(36) Boonluksiri, Y.; Prapagdee, B.; et al. Effect of poly(D-lactic acid) and cooling temperature on heat resistance and antibacterial performance of stereocomplex poly(L-lactic acid). *J. Appl. Polym. Sci.* **2020**, *137*, 48970.
(37) Tsuji, H.; Ikada, Y. Stereocomplex formation between enantiomeric poly(lactic acid)s. XI. Mechanical properties and morphology of solution-cast films. *Polymer* **1999**, *40*, 6699−6708.

https://doi.org/10.1021/acsomega.1c07025
ACS Omega 2022, 7, 22149−22160